MALEDI, N.B., POTGIETER, J.H., SEPHTON, M., CORNISH, L.A., CHOWN, L. and Süss, R. Hot corrosion behaviour of Pt-Alloys for application in the next generation of gas turbines. *International Platinum Conference 'Platinum Surges Ahead'*, The Southern African Institute of Mining and Metallurgy, 2006.

Hot corrosion behaviour of Pt-Alloys for application in the next generation of gas turbines

N.B. MALEDI[*†], J.H. POTGIETER[*§], M. STEPHTON[*], L.A. CORNISH[†§], L. CHOWN[†§] and R. SÜSS[†§]

[*]*School of Process and Materials Engineering, University of the Witwatersrand*

[†]*Advanced Materials Division, Mintek*

[§]*DST/NRF Centre of Excellence for Strong Materials, University of the Witwatersrand*

In today's gas turbines, the emphasis is on saving energy and reducing the amounts of pollutants emitted. This can be attained only by designing alloys with higher melting points and the capability to retain mechanical integrity at increased temperatures. The development of nickel-based superalloys (NBSAs) has reached its limit, as the alloys are operating at critical temperatures close to their melting points. Further increase in the operating temperatures will result in dissolution of the strengthening phases and even melting. Recent trends are towards developing materials that are adequately strong but have much higher melting points and corrosion resistance than the NBSAs that are currently in use. Studies conducted on Pt alloys with similar structure to the NBSAs have presented mechanical results that are promising. This has led to further development of these alloys as a replacement for NBSAs. The operations of gas turbines are usually limited by hot corrosion, which could lead to catastrophic failures. Increased temperatures have an adverse effect on the corrosion of the alloys by making the environment more aggressive. Hence, during a material selection process, the corrosion behaviour of any selected material for a highly specialized application such as gas turbines needs to be assessed. Generally, coatings are applied to combat degradation by salt deposits, hence coated and uncoated NBSAs were selected as benchmark alloys. Corrosion mechanisms and kinetic studies of the Pt alloys were conducted. High temperature hot corrosion (HTHC) tests were conducted at 950°C for 540 hours. Analysis of the corrosion products was conducted using a Raman spectrometer, scanning electron microscope with energy dispersive X-ray spectroscopy (EDS) optical microscopy, and X-ray diffraction study of the phases that formed. Both coated and uncoated NBSAs failed under the test conditions. Samples were covered with a porous non-adherent greenish layer which is characteristic of NiO. Pt alloys displayed superior corrosion properties compared with the benchmark alloys.

Introduction

Superalloys are engineering materials used in demanding applications such as industrial waste incinerators, the power generation industry, chemical processing, pulp and paper production, and land and aeroplane gas turbines[1, 2]. Nickel-based superalloys (NBSAs) find their largest application in the gas turbine industry[1], constituting over 50% of the gas turbine weight. NBSAs are preferred because of the alloys' superior mechanical strength, surface stability, creep and fatigue resistance[3]. Early age gas turbines were developed after the 1940s, and were designed to operate at 700°C. Improvements in metallurgical processes, blade cooling techniques and application of coatings allowed for increased working temperatures[4]. Coatings made a greater contribution towards increased temperatures and protection against environmental degradation[5, 6]. Today, the fourth generation gas turbines (single crystal alloys containing ruthenium) are operating at 1 100°C. Furthermore, temperature increases to 1 350°C are desirable to improve the performance of gas turbines, reduce fuel consumption and comply with the stringent criteria of environmental legislation[3, 6].

It would be advantageous for gas turbines to be operated at increased temperatures. However, the projected temperatures are excessively high for NBSAs. Hence, novel higher melting point materials with better mechanical (creep, fatigue, and strength) and chemical (oxidation and hot corrosion) properties were developed to replace those currently used[6,7]. Possible candidate materials with higher melting points, such as ceramics, intermetallics, refractory metals and composites were considered for gas turbine applications[2]. However, these materials, excluding the latter, have limitations that prevent them from being used in high temperature applications[8].

Another group of materials considered was the platinum group metals (PGMs) [Pt, Pd, Ir and Rh]. Amongst this group, Pt-based alloys were further developed and evaluated because they have a fcc crystal structure similar to that of NBSAs, higher melting points and good corrosion resistance[9]. In addition, Pt alloys can be used in demanding applications such as glass manufacturing and handling of corrosive elements[10]. Pt as an additive in coatings exhibited superior resistance against hot corrosion attacks, and today Pt-modified coatings are preferred for resistance against

Type I hot corrosion in gas turbines[11,12,13]. Nonetheless, Pt has its disadvantages, such as its high cost and high density. Regardless of the high cost of Pt, there would be greater benefits for both the mining and the aerospace industry if more platinum was used. The use of Pt in the gas turbine industry would allow for saving of cost in fuel and coatings, and Pt can be reprocessed and recycled. It is anticipated that the Pt-alloys could be used in any high temperature application, where strength and/or corrosion resistance is desirable, other than the aerospace industry.

Creep and high temperature corrosion are the two principal degradation factors that contribute towards failure of most gas turbines[6,11]. Hence, it important that during the materials selection process, high temperature corrosion be evaluated as a selection criterion, and that the chosen material has adequate properties for the application. Creep and oxidation studies of the developed alloys were studied at Mintek. The findings by Süss *et al.*[7] were very encouraging, and therefore hot corrosion properties were further evaluated.

Hot corrosion is the degradation of high temperature materials in the presence of molten sodium sulphate[14]. The source of sodium sulphate could be the ingested air or impurities in fuels used. Hot corrosion has detrimental effects on the mechanical integrity of the alloys, and excessive attacks could result in catastrophic failures[14]. Increased temperatures also have an adverse effect leading towards hot corrosion[2,15]. There are two forms of hot corrosion, namely Type I, also known as high temperature corrosion (HTHC), which occurs at temperature ranges between 850–950°C, with the conditions being more aggressive at 900°C. Type II or low temperature hot corrosion (LTHC), occurs at temperature ranges of 650–800°C[4]. It is Type I hot corrosion that occurs mostly in gas turbines, hence the evaluation focused on this type of corrosion.

This work deals with the hot corrosion behaviour of Pt-alloys. Weight gain measurements were employed to assess the corrosion kinetics of the alloys. The study examined the effect of alloying elements towards corrosion resistance and the corrosion mechanisms were studied.

Experimental procedure

The high temperature corrosion behaviour of Pt-alloys was studied by performing a crucible test. The test was conducted at 950°C to increase the corrosion kinetics. This temperature was selected because it is within the temperature ranges at which hot corrosion is most effective. Seven samples were prepared by grinding on silicon paper to 1 000 m finish and degreased by rinsing in acetone. Five of these specimens were Pt-alloys and the other two samples were benchmark alloys. Samples were covered in analytical anhydrous Na_2SO_4 salt, which acted as the corrosive electrolyte inside a 20 ml high alumina crucible that was placed inside a Townson and Mercer furnace in a static dry air environment.

The test was performed for 540 hours, with an initial 60 cycles of 1 hour of heating and 20 minutes of cooling to room temperatures, followed by subsequent long cycles of 72 hours of heating. The samples were cleaned by dipping them in boiling distilled water. Samples (free of salt residues) were weighed at the end of every cycle on a Mettler Toledo weighing balance, which has a sensitivity of 0.1 mg. Fresh salt was provided for every cycle. The corrosion morphology and the cross-sectional analysis of the corroded alloys were studied by characterization with techniques such as the scanning electron microscopy (SEM) with energy dispersive spectrometer (EDS), X-ray diffraction (XRD), Raman spectroscopy and optical microscopy (OM).

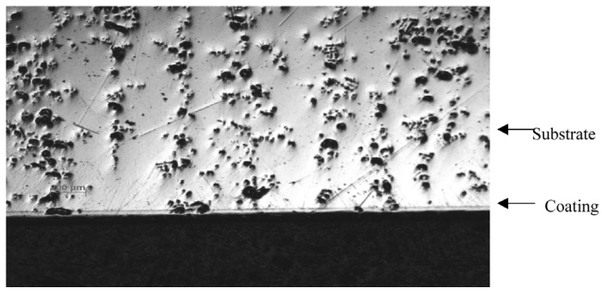

Figure 1. Optical micrograph of the coated NBSA sample in the as-polished condition showing the protective coating

Investigated alloys

Pt-alloys

Five Pt-based alloys with different chemical compositions were selected from the programme[10] and manufactured at Mintek for the investigation. The samples were made from elements of 99.9% impurities and melted in a button-arc furnace under argon, on a water-cooled copper hearth. They were turned several times for improved homogeneity. The chemical compositions are given in Table I.

Benchmark alloys

Two single-crystal nickel-based superalloys (NBSAs) were used as benchmark alloys in the study. A thin platinum aluminide coating, [Pt_2Al (at. %: 67Pt, 33Al)] of approximately 1.25 μm thickness was deposited on one of the benchmark alloys, whilst the other alloy was left uncoated. Table II gives the chemical composition of CMSX-4, the single crystal alloy, and Figure 1 illustrates the thickness of the coating.

Materials characterization

Samples were prepared for metallography (cut, mounted and polished). Four characterization techniques were

Table I
Nominal chemical composition of selected Pt-based alloys (at. %).

Alloy	Pt	Al	Cr	Ru	Co
RS-1	86	10	4	-	-
RS-2	86	10	-	4	-
RS-3	84	11	3	2	-
P420	79	15	-	-	6
P421	73	15	-	-	12

Table II
Nominal chemical composition of CMSX-4 (wt.%).

Alloy	Ni	Cr	Co	Mo	W	Ta	Al	Ti
CMSX-4	Balance	5.7	11	0.42	5.2	5.6	5.2	0.74

employed to study and evaluate the corrosion mechanism of the investigated alloys.

Crucible test

For the initial crucible test, thin discs of the samples were placed in alumina crucibles, covered in Na_2SO_4 and placed in a furnace at 900°C for 168 hours. The samples were weighed every 24 h, and the mass change recorded. The corroded surface was examined in a SEM, and the corrosion product was analysed using XRD.

Optical microscopy

An Axiocam microscope installed with the Axio ver. 3.1 programme was used to study the cross-sections of the corroded samples.

Scanning electron microscopy (SEM with EDS)

A JEOL 840 scanning electron microscope was used to study the different corroded morphologies, in plan and in cross-sections of the alloys, using an accelerating voltage of 20 keV. Quantitative and qualitative analyses were undertaken using energy dispersive X-ray spectroscopy (EDS) connected to the SEM unit.

X-ray diffraction (XRD)

A Phillips-PW1710 XRD was used to identify corrosion products that formed on the surfaces of the seven alloys. The generator settings for the analysis were set at 40 kV and 20 mV with copper K-alpha as the anode. A scan with a step size of 0.02° per minute was run from a starting position of $2\theta = 10°$ up to $2\theta = 100°$. The Expert High Score software was used to identify peaks of the spectra.

Raman spectroscopy analysis

Raman spectroscopy (JOBIN-YVON T64000) was used to identify thin surface films on the samples. The spectrum was collected by directing a continuous laser of Ar^+ (514.5 nm) on the alloy surface at room temperature. The spectrum covered a scanning range between 250 cm^{-1} and 2 500 cm^{-1}. The peak positions were compared with those in the literature to identify the different compounds found [17].

Results

Mass gains from the crucible test

The mass gains of the samples from the crucible test of being immersed in Na_2SO_4 at 900°C for 168 hours are given in Table III and Figure 2. After day 3, the tests on the uncoated CMSX-4 specimen were discontinued. It can be seen that there was very little change in mass for the Pt-based alloys, as a result of the formation of the protective scale. In the case of the uncoated NBSA, initial mass gain was as a result of the formation of oxides, and further reactions and the formation of un-protective oxides resulted in catastrophic corrosion which led to change in mass. The test was discontinued as the uncoated sample degraded. XRD analysis of the product showed a mixture of compounds based mainly on sodium, and nickel. Conversely, for the Pt-based alloys, XRD showed that the surface was mainly alumina, which is the oxide coating that forms naturally. This was a good indication that the Pt-based substrate was supporting the alumina layer well. The morphologies of the Pt-based alloys were much better than those of the NBSA. RS-1 (Pt-Al-Cr) had the best appearance, and RS-3 (Pt-Al-Cr-Ru) and RS-2 (Pt-Al-Ru) were slightly pitted, with the latter showing more pits. P420 (Pt-Al-6Co) appeared good in places, with losses in other places. However, it must be realised that these pits are small in nature, and negligible when compared with the damage to the NBSA. With the naked eye, no change in appearance could be seen in the Pt-based alloys. The data are shown in Figure 2.

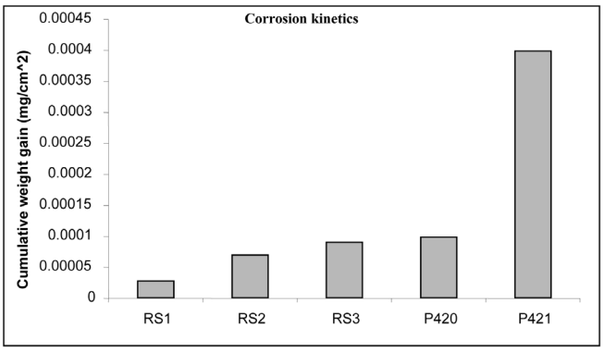

Figure 2. Comparison of mass losses after the crucible test at 950°C

Corrosion kinetics

Alloy P421 obeyed a linear behaviour, with continuous weight gain throughout the experiment. The alloy had the highest weight gains compared with the other alloys that were evaluated. Alloy RS-1, which showed the lowest weight gain accumulated weight during the first 72 hours. The mass remained constant until 300 hours elapsed, ie. there were no further weight gains. Alloys RS-2, RS-3 and

Table III
Mass gain of the samples at 900°C in the crucible test: immersed in Na_2SO_4 at 900°C for 168 hours.

Sample	Mass (g)						
	Initial	Day 1	Day 2	Day 3	Day 4	Day 5	Day 6
Pt86:Al10:Cr4	0.611	0.613	0.612	0.611	0.612	0.612	0.612
Pt86:Al10:Ru4	0.478	0.477	0.478	0.479	0.479	0.479	0.478
Pt84:Al11:Cr3:Ru2	0.522	0.524	0.523	0.524	0.522	0.522	0.522
Pt79:Al15:Co6	0.600	0.600	0.600	0.600	0.601	0.601	0.601
Pt15: Al15:Co12	0.663	0.665	0.668	0.668	0.667	0.672	0.675
Uncoated CMSX-4	4.430	4.431	4.596	4.583	-	-	-

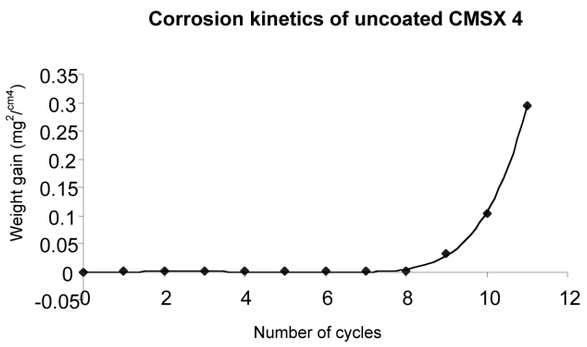

Figure 3. Corrosion kinetics of the uncoated NBSA after exposure from Na_2SO_4

P420 had intermediate weight gains. The corrosion rate constants (Table IV) indicated that alloy RS-1 had the lowest corrosion kinetics, whilst alloy P421 was the most reactive alloy amongst the alloys investigated. These constants were calculated by fitting data through a parabolic equation and using the method of least squares to calculate the values of the constants.

Figure 3 illustrates the corrosion kinetics of the uncoated NBSA, which failed after 11 hours, following an exponential rate law. Greater mass gains were accumulated during the propagation stage, which happened within a short period. At this stage, the sample was removed from the test. The non-protective scale that formed was green in colour and very brittle.

Figure 4 shows the corrosion behaviour of the coated NBSA which followed a parabolic rate law. The alloy showed better resistance than the uncoated NBSA because the coating protected the alloy from degradation, by separating it from the environment.

Table IV
Corrosion rate constants of Pt-based alloys.

Alloys	K_p ($g^2cm^{-4}s^{-1}$)
RS-1	3.99×10^{-14}
RS-2	2×10^{-13}
RS-3	2.2×10^{-13}
P420	2.2×10^{-13}
P421	$*8.52 \times 10^{-8}$

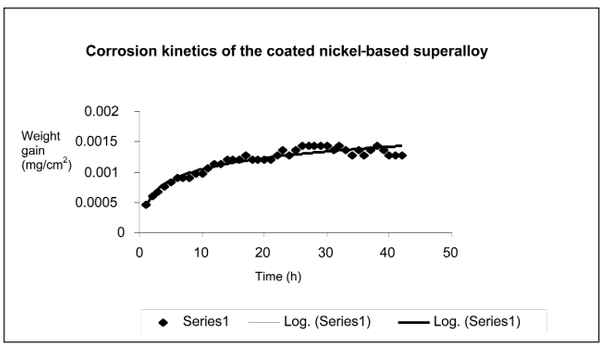

Figure 4. Corrosion kinetics of the coated NBSA after exposing to hot corrosion

The corrosion kinetics followed by Pt-based alloys were similar to each other and different from those of the NBSAs. There were greater variations throughout the duration of the experiments, especially with alloys P420 and P421 (the alloys with Co additions) showing instabilities. Alloys RS-1 and RS-3 lost weight within the first four hours of exposure; samples tried to reach stability after the sixth cycle.

Corrosion morphologies

Figures 6–12 show the corrosion morphologies that resulted when the samples were exposed to molten sodium sulphate salt at 950°C. It was evident that both coated and uncoated NBSAs suffered greater attack than the Pt-based samples, forming a non-protective porous scale. Figures 5 and 6 show the corroded morphologies of the two NBSA samples. Figure 5 shows that the coating broke up and thus gave no protection. In Figure 6, the crack on the surface of the uncoated NBSA shows the brittleness of the corrosion product formed. The corrosion morphology explains why these alloys had higher corrosion kinetics.

The corroded morphology of alloy P421 (Pt-Al-12Co) showed a disintegrated scale layer (Figure 8). This morphology indicates that scale was not protective in this environment, allowing for easy diffusion of elements from

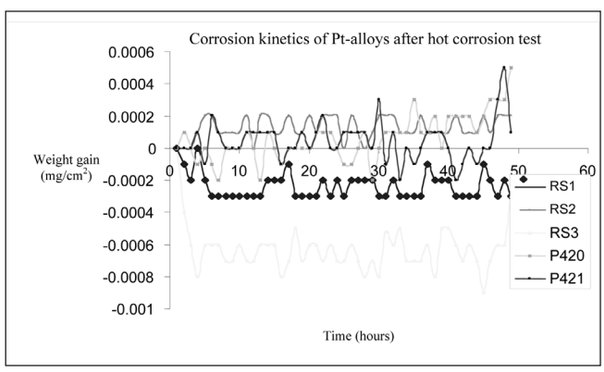

Figure 5. Corrosion kinetics of five Pt-alloys of various chemical compositions

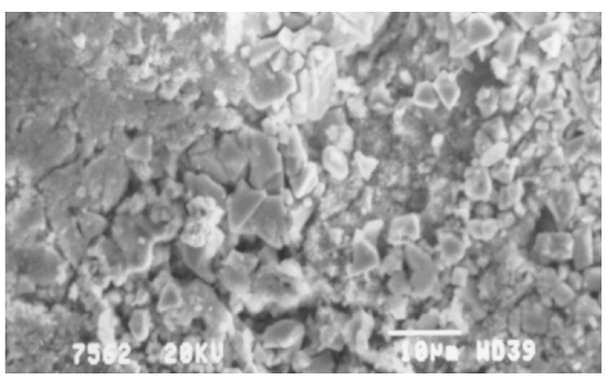

Figure 6. SEM secondary electron image showing the corroded morphology of the coated NBSA that resulted after reacting with molten sodium sulphate salt at 950°C

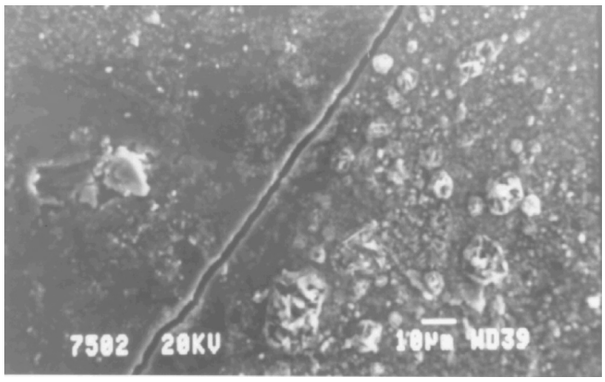

Figure 7. SEM secondary electron image of the corroded morphology after exposing the uncoated NBSA to molten sodium sulphate salt at 950°C, showing a crack in the brittle and non-protective scale that was formed

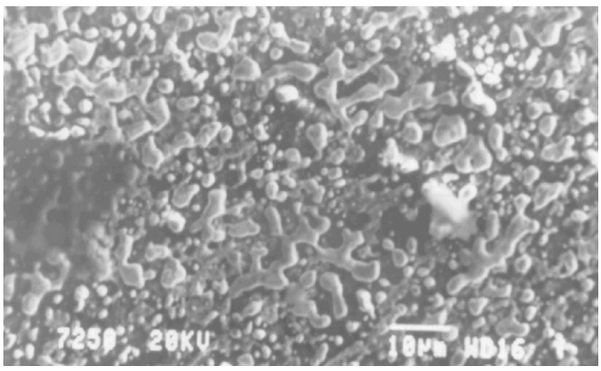

Figure 8. SEM secondary electron image showing the non-protective oxide scale that formed on the surface of alloy P421: Pt-Al-12Co

the substrate to the metal-salt interface and vice versa.

The other alloy with cobalt, P420 (Pt-Al-6Co) showed a similar corroded morphology, as shown in Figure 9.

The scale morphologies of alloys RS-1 (Pt-Al-Cr), RS-2 (Pt-Al-Ru) and RS-3 (Pt-Al-Cr-Ru) presented in Figures 10–12 are slightly similar. The morphologies were more tenacious and complete, although apparently porous, and

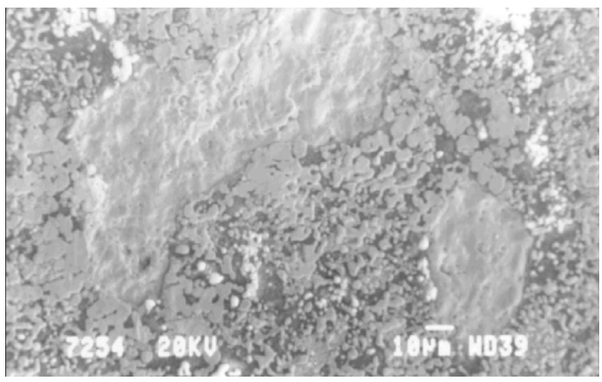

Figure 9. SEM secondary electron image showing the corroded morphology of alloy P420 (Pt-Al-6Co) after exposure to molten sodium sulphate salt

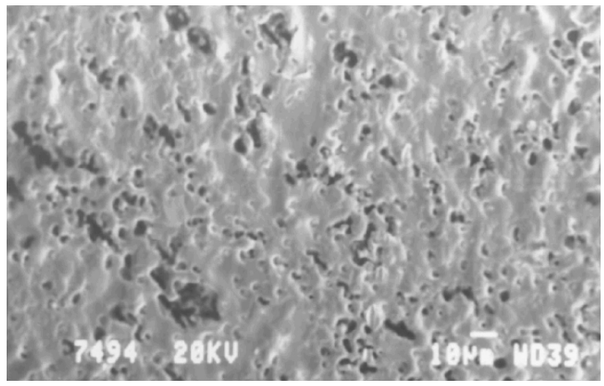

Figure 10. SEM secondary electron image showing the porous oxide scale that formed on the surface of alloy RS-1 (Pt-Al-Cr) after exposure to molten sodium sulphate

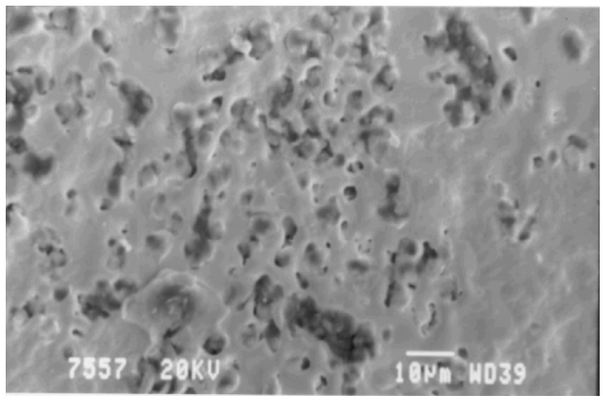

Figure 11. SEM secondary electron image showing the corrosion morphology after alloy RS-2 (Pt-Al-Ru) was exposed to molten sodium sulphate

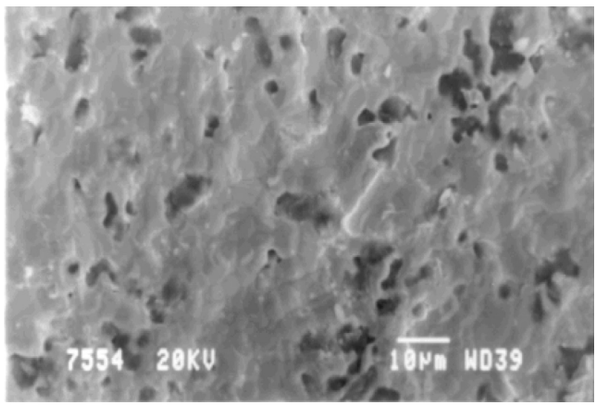

Figure 12. SEM secondary electron image showing the corrosion morphology of alloy RS-3 (Pt-Al-Cr-Ru) after 540 hours exposure to molten sodium sulphate

gave more protection against hot corrosion than in the Pt-based alloys with cobalt.

Cross-sectional analysis

SEM and optical microscopy techniques were employed in

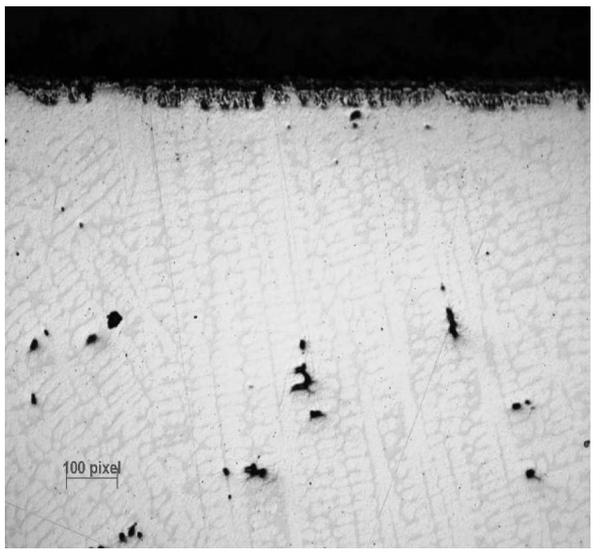

Figure 13. Optical micrograph showing the cross-section of alloy RS-3 (Pt-Al-Cr-Ru)

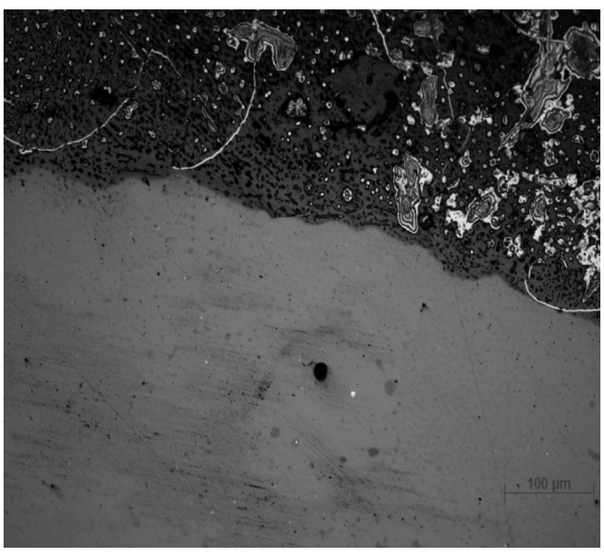

Figure 14. Optical micrograph showing the cross-section of alloy P421 (Pt-Al-12Co) at 20X magnification

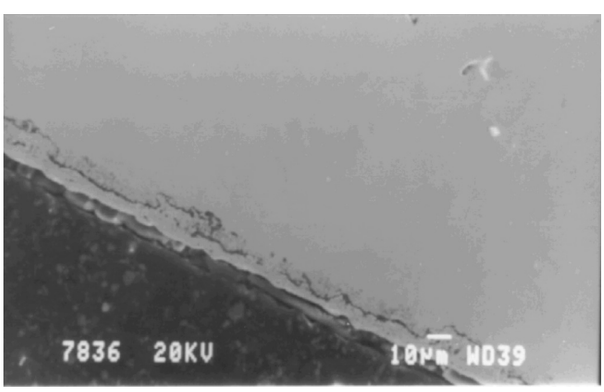

Figure 15. SEM secondary electron image showing the thin protective scale on the surface of alloy RS-1 (Pt-Al-Cr)

analysing the cross-sections of the alloys in order to estimate the depth and degree of the attack. Figures 13 and 14 show the difference of the extent of attack between two Pt-based alloys: RS-3 (Pt-Al-Ru) and P421 (Pt-Al-12Co). The results show that under similar conditions, alloy P421 suffered greater attack.

The SEM micrographs revealed that there was a very thin oxide film on the surface of alloys RS-1 (Pt-Al-Cr), RS-2 (Pt-Al-Ru) and RS-3 (Pt-Al-Cr-Ru), which was not visible using optical microscopy. Although this scale rendered protection against high temperature corrosion, the porous structure did allow some internal attack, as depicted in Figures 15–17, and to depths of about 15 µm beneath the scale for all the Pt-based alloys without Co.

XRD analysis

X-ray diffraction analysis of the corroded samples was used to identify the corrosion products formed on the surface of the corroded samples. The corrosion product compounds for which peaks were identified are summarised in Table V, with the most likely compounds being marked with an asterisk, and one example of an XRD spectrum is presented in Figure 18. Since many of the peaks were identified as belonging to more than one phase, interpretation had to be done to select the compounds most likely to corrode. The most likely phases are those with many matched peaks, especially including peaks that were not matched to other

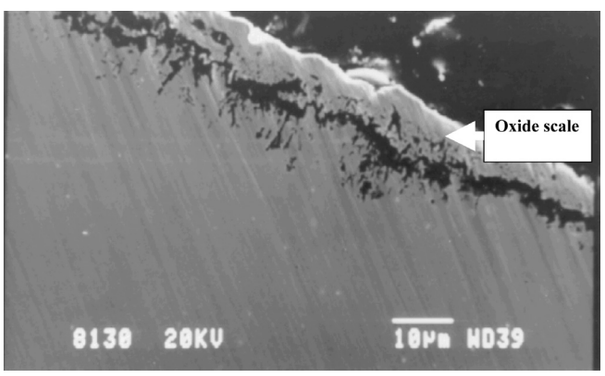

Figure 16. SEM secondary electron micrograph showing the oxide scale on the surface of alloy RS-2 (Pt-Al-Ru)

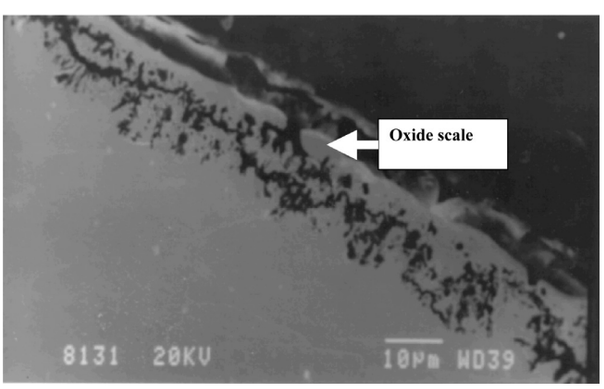

Figure 17. Secondary electron image showing the scale on the surface of alloy RS-3 (Pt-Al-Cr-Ru)

compounds. As some of the peaks were matched to more than one compound, those with only one occurrence are less likely. Those without an asterisk are considered less likely, because they always matched with another compound that had its own unique peaks. At this stage, the peak heights have yet to be compared to ascertain whether more than one peak is superimposed. Some peaks in all of the samples were also unidentified. Figure 15 shows that the salt reacted with the RS-1 (Pt-Al-Cr) sample, forming Na-compounds. It is likely that Cr-oxides, Al-oxides and Pt-oxides further reacted with the salt to form the compounds that were detected during the analysis. The corrosion compounds formed on the surface of alloy RS-2 (Pt-Al-Cr) show that, amongst other compounds, Al_2O_3 did form on the surface of the alloy. Where Pt_3Al was found, it could have been the phase in the substrate below. Na_2SO_4 was detected on the surface of alloy RS-3 (Pt-Al-Cr-Ru), with other desired compounds such as Al_2O_3, which is believed to protect the alloy against high temperature attacks. Elemental sulphur was detected on the surface of alloy P420 (Pt-Al-6Co), which indicated that at high temperature Na_2SO_4 acted as a source of sulphur to form internal attacks on the surfaces of the alloy. There was the possibility of cobalt oxides forming. During the experiments on the alloys comprising cobalt, it was observed that Co diffused from the metal sample, leaving blue colourings inside the crucible. These were identified as Co_3O_4 by XRD analysis.

Not surprisingly, different potential corrosion products were determined by XRD, and these are given in Table VII, again with an asterisk denoting the more likely compounds. The NBSAs formed a green corrosion product. The corrosion products comprised mostly NiO and spinels, and molybdenum oxides were also detected. Results were supported by SEM/EDX analysis. Figures 19–20 represent some of the spectra obtained from corroded samples.

Table V
Summary of the potential corrosion products in the Pt-based alloys as detected by XRD.

RS-1 (Pt-Al-Cr)	RS-2 (Pt-Al-Ru)	RS-3 (Pt-Al-Cr-Ru)	P420 (Pt-Al-6Co)	P421 (Pt-Al-12Co)
Na_5AlO_4 *	Pt_3O_4	Na_2SO_4 *	Na_2SO_4 *	$CoSO_4$ *
$Na_2Cr_2O_7$ *	NaO_4Pt_3	Na_2CrO_4 *	S *	Na_2SO_4 *
Na_2O	Na_2SO_4	Al_2O_3 *	Al_2O_3 *	$NaPt_3O_4$ *
$NaPt_3O_4$ *	$NaAl_5O_4$ *	Pt_3O_4	Na_2O *	Co_3O_4 *
Pt	O_2Ru	Na_2O	$NaPt_3O_4$	
Pt_3O_4	Na_2O	$AlNaO_2$ *	$CoSO_4$	
	$AlNaO_2$ *	Pt_3Al	Pt_3Al *	
	Al_2O_3 *		Pt_3O_4	
	Al_3Ru2		CoO	
	Pt_3Al *		Co_3O_4	

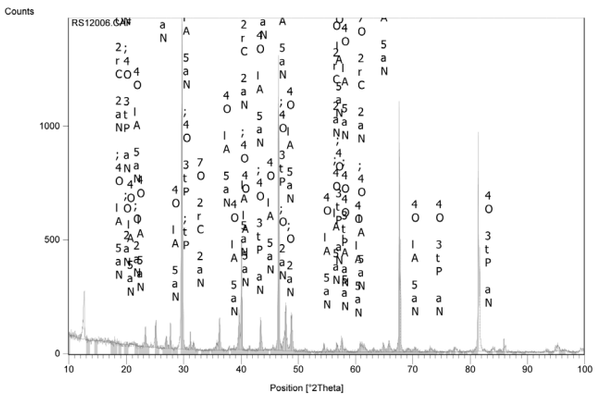

Figure 18. XRD spectrum showing the corrosion products on the surface of alloy RS-1 (Pt-Al-Cr) after exposure to molten sodium sulphate salt at 950ºC

Table VI
Summary of the potential corrosion products in the NBSAs as detected by XRD.

RS-1 (Pt-Al-Cr)	RS-2 (Pt-Al-Ru)	RS-3 (Pt-Al-Cr-Ru)	P420 (Pt-Al-6Co)	P421 (Pt-Al-12Co)
Na_5AlO_4 *	Pt_3O_4	Na_2SO_4 *	Na_2SO_4 *	$CoSO_4$ *
$Na_2Cr_2O_7$ *	NaO_4Pt_3	Na_2CrO_4 *	S *	Na_2SO_4 *
Na_2O	Na_2SO_4	Al_2O_3 *	Al_2O_3 *	$NaPt_3O_4$ *
$NaPt_3O_4$ *	$NaAl_5O_4$ *	Pt_3O_4	Na_2O *	Co_3O_4 *
Pt	O_2Ru	Na_2O	$NaPt_3O_4$	
Pt_3O_4	Na_2O	$AlNaO_2$ *	$CoSO_4$	
	$AlNaO_2$ *	Pt_3Al	Pt_3Al *	
	Al_2O_3 *		Pt_3O_4	
	Al_3Ru2		CoO	
	Pt_3Al *		Co_3O_4	

Table VII
Summary of the potential corrosion products in the NBSAs as detected by XRD.

Uncoated NBSA	Coated NBSA
MoO_3 *	NiO
$Ni(Cr_2O_4)$ *	$NiAl_2O_4$ *
$NiAl_2O_4$	TiO_2 *
$NiMoO_4$ *	$NiCr_2O_4$ *
NiO	
MoO_2	

Raman analysis

Figure 21 illustrates the results obtained using the Raman analysis, which suggested that the peaks represented the

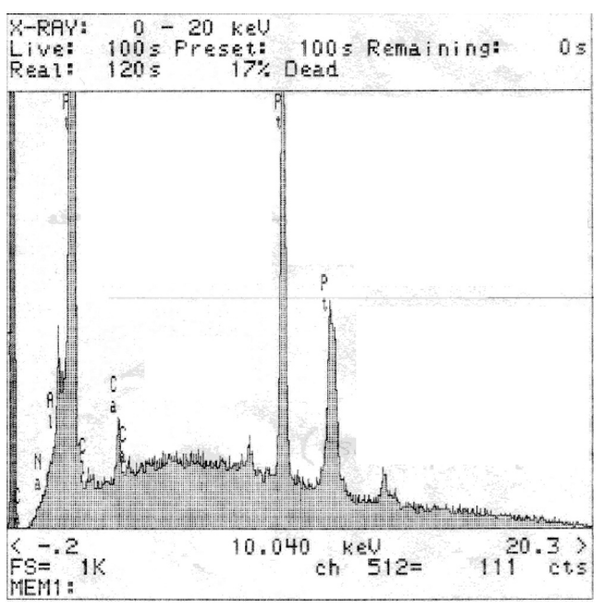

Figure 19. SEM/EDX spectrum of the corroded surface area of the uncoated NBSA

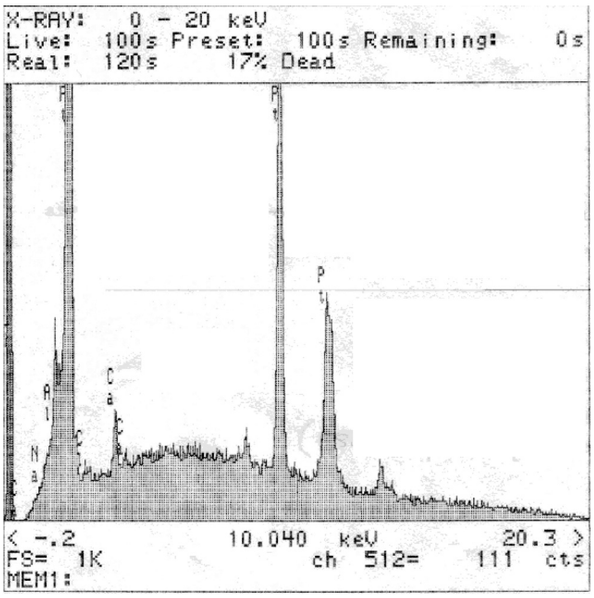

Figure 20. EDX spectrum obtained from the corroded surface area of alloy RS-1 (Pt-Al-Cr)

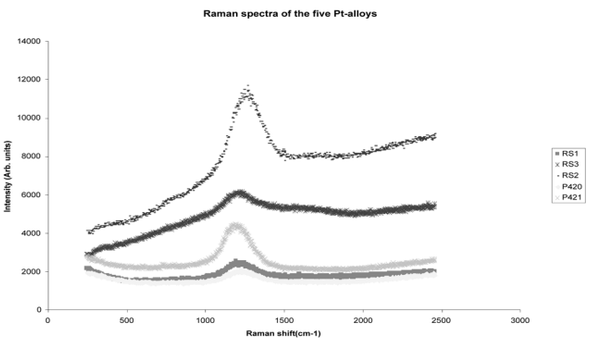

Figure 21. Raman analysis of the corroded surface of the Pt-based alloys

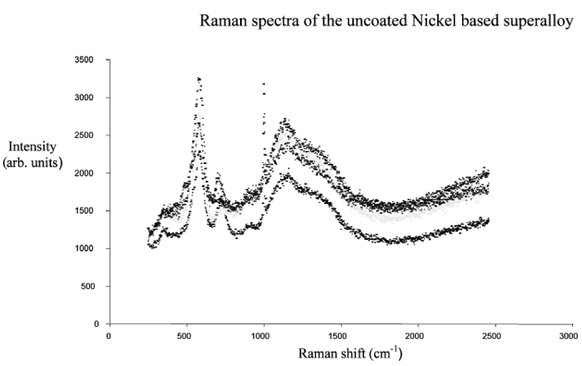

Figure 22. Raman analysis of the corroded uncoated NBSA

Table VII
Peak positions (cm^{-1}) identified as NiO obtained from Raman spectra on surface of the uncoated NBSA.

NiO	This work	Reference[17]
	1155	1074
	917	910
	727	725
	585	532
	367	400

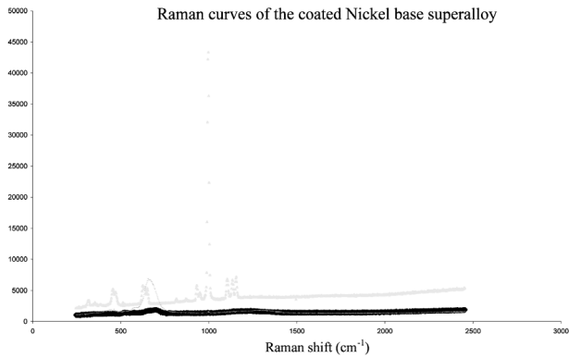

Figure 23. Raman spectra of the uncoated NBSA after exposing the alloy to molten sodium sulphate

presence of trace Na_2SO_4[16]. These results were also confirmed by most of the alloys' XRD analysis.

The Raman spectrum of the uncoated NBSA is given in Figure 22, and the peak matches are shown in Table VIII. The literature was again used to identify the compound and the results matched with those of NiO[17], but it can be seen (in Table VIII) that the first peak was a poor match. The peaks of NiO were also matched in XRD, but not uniquely. Similar results were obtained for the uncoated NBSA at relatively low intensities, and the results are presented in Figure 23.

Discussion

High temperature materials rely on the formation of a slow-growing oxide scale for protection against high temperature corrosions[11]. Cr and Al oxides are preferred for protection against high temperature corrosion. Aluminium forms slow-growing oxides which do not volatilize, whereas Cr_2O_3 are limited to temperatures below 850°C [13].

The investigated Pt-based alloys and the NBSAs reacted differently to high temperature hot corrosion. The Pt-based alloys displayed much better corrosion resistance, with low mass losses within the range of 0.0002–0.0008 mg/cm^2, whilst NBSAs had the highest mass gain.

The single crystal CMSX-4 alloy is susceptible to hot corrosion, hence coatings are applied to most of the NBSAs when used in gas turbines. This was confirmed by the fast corrosion kinetics observed for the uncoated NBSA in this study. The uncoated NBSA failed prematurely in the early stages of the experiment, gaining voluminous weight of a green corrosion product, as described by Eliaz *et al.*[4] as an indication of the occurrence of Type I hot corrosion. Similar behaviour was observed in the coated NBSA after 540 exposure hours. The corrosion product of NBSAs consisted mainly of NiO and Ni $(AlCr)_2O_4$ spinels, as detected by XRD, and confirmed by SEM (for the elements

involved) and Raman analysis.

Corrosion of the uncoated NBSA obeyed an exponential rate law, whilst the coated NBSA followed a parabolic rate law. This agreed with the knowledge that coated NBSAs are able to withstand high temperatures for a longer time owing to the presence of the protective coating, which acts as a barrier, minimizing the rate of interaction between the corrosive medium and the alloy [18].

Pt-based alloys showed better resilience against corrosion attack, with low corrosion kinetics. The initial weight losses observed in alloys RS-1 and RS-3 might be due to the formation of further oxides of CrO_3 governed by the following reaction:

$$2CrO_3 \rightarrow Cr_2O_3 + 3/2O_2$$

Spalling starts as the result of continued reaction between O_2 and Cr_2O_3. However, more work is required to support this assumption. Lower weight gains and slight physical changes implied that the alloy remained at the incubation stage for a prolonged period, without going through the propagation stage.

Many other high temperature materials undergo long incubation periods. Nonetheless, this does not mean the alloys used in this case are immune to corrosion attacks[18]. When analyzing the cross-sections of Pt-based alloys, it was observed that the alloys suffered internal attacks, with depletion of the alloying elements. This is usually owing to the influence of sulphur. However, sulphur was not detected by the EDS analyses, owing to both low concentrations and low detection limits (approximately 1 wt.%); hence other characterization techniques were utilized to explain the corrosion products, and determine the corrosion mechanism in the Pt-based alloys.

NBSAs are believed to fail in two degradation stages, with the two main mechanisms being fluxing and sulphidation[19]. Similar findings were made in this study. The fluxing and sulphidation mechanisms led to failure of the alloys, and penetration of sulphur was observed.

Alloying elements have a significant role in providing resistance to high temperature corrosion. Mo in NBSAs is used as a solid solution strengthener, but renders the alloy more susceptible to hot corrosion attacks. The formation of MoO_3, as detected by XRD analysis, leads to acidic fluxing of the alloy [8].

The corrosion mechanism of the Pt-alloys is assumed to be fluxing of the protective scale, as observed with the corrosion morphologies and the cross-section of alloy RS-3 (Pt-Al-Cr-Ru) in Figure 17. The depletion of alloying elements in other sections of the alloys is still unexplained, even though it is understood that some of the loss in these elements is due to the formation of volatile compounds.

Despite the fact that the Pt-based alloys exhibited much higher resistance compared with NBSAs, the different compositions led to various corrosion behaviour in the Pt-based alloys. Alloys RS-1 (Pt-Al-Cr), RS-2 (Pt-Al-Ru) and RS-3 (Pt-Al-Cr-Ru) have a better potential for use in aggressive environments, because of the stable oxides that were formed. The level of attack and penetration by foreign elements was negligible compared with their effect on the other alloys investigated. This corrosion resistance is attributable to the formation of the protective scale, even though internal attack did occur. Good corrosion resistance is assumed to be due to the platinum itself, and its inherent stability. The other alloying elements, such as Al and Cr, make a significant contribution towards hot corrosion. The presence of Cl as a trace element in the analytical salt contributed to the formation of pits on the surface of alloy RS-1, and this is illustrated in Figure 24. Pits are common in Type II hot corrosion.

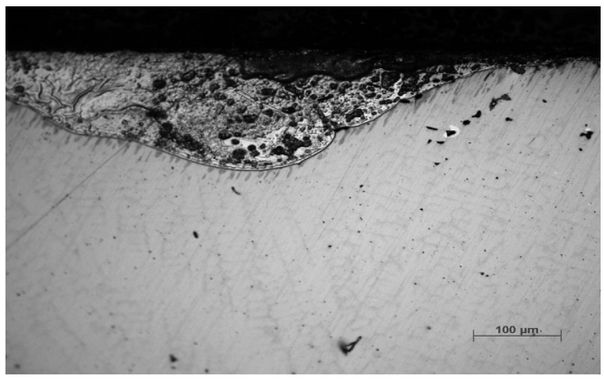

Figure 24. Optical micrograph showing pits on the surface of alloy RS-1 (Pt-Al-Cr) that formed during the exposure to Na_2SO_4 salt at 950ºC.

Co-based alloys are known to have better corrosion resistance than NBSAs[5]. In the research programme[10], Co was added to Pt-alloys to improve formability of the alloys, although the results of this investigation showed that Co additions were not beneficial for corrosion resistance, and the results of the other Pt-based alloys were better. These Co-containing alloys showed greater degradation, with more disrupted corrosion morphologies, and greater penetrations below the protective scale. Cracks formed on the surface of alloy P420 (Pt-Al-6Co), as shown in Figure 25. It was thought that the cracks could have been initiated by thermal stresses, or was caused by the penetration of sulphur, as detected by XRD analysis. The formation of cracks by alloy P420 (Pt-Al-6Co) limits its applications for high temperature corrosion, since crack resistance is also one of the properties required in high temperature applications.

Conclusions

Experiments were undertaken in molten sodium sulphate on five different Pt-based alloys, and coated and uncoated NBSAs. Results showed that:

- the formation of thin scale on the surface of the three alloys makes the alloys more resistant

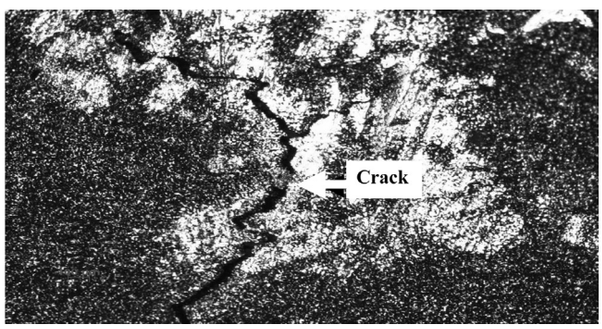

Figure 25. Corroded surface of alloy P420 (Pt-Al-6Co) with a crack

- fluxing of the protective scale resulted in the alloys being more susceptible to attacks at high temperatures
- alloys RS-1, RS-2 and RS-3 showed better corrosion resistance, outperforming the coated and uncoated NBSAs; which is very encouraging for the development of Pt-based alloys for applications in gas turbine engines
- Pt was beneficial in the bulk alloys, and similar behaviour was observed in Pt-based alloys, where Pt together with Al and Cr were found to significantly improve the corrosion resistance, as shown by alloys RS-1 (Pt-Al-Cr), RS-2 (Pt-Al-Ru) and RS-3 (Pt-Al-Cr-Ru)
- the Pt-based alloys with Co performed much better than both NBSAs, but were not as stable as the Pt-based alloys with Cr and Ru, owing to the formation of Co oxides, which are more volatile.

Future work and recommendations

The corrosion behaviour of Pt-based alloys in sulphur-containing gaseous environments also needs to be assessed. The effect of sulphur on the corrosion mechanism governing failure of the Pt-based alloys is still to be investigated.

Acknowledgements

The financial assistance of the South African Department of Science and Technology (DST), the Platinum Development Initiative (PDI) and the DST/NRF Centre of Excellence is gratefully acknowledged.

This paper is published with the permission of Mintek.

References

1. SIMS, C.T., CHESTER, T., STOLOFF, N.S. and HAGEL, W.C. *Superalloys II*. John Wiley and Sons Inc. 1972.
2. ELLIOT, P., Practical Guide to High Temperature Alloys. Nickel Development Institute. pp. 1–10. 1990.
3. SALTYKOV, P., FABRCHNAYA, O., GOLCZEWSKI, J. and AlDINGER, F. Thermodynamic modeling of oxidation of Al-Cr-Ni alloys. *J. Alloys and Compounds*, vol. 381. 2004. p. 99.
4. ELIAZ, N., SHEMESH, G. and LATANISION, R.M. Hot corrosion in gas turbine components. *Engineering Failure Analysis*, vol. 9, issue 1. 2002. pp. 31–43.
5. STRINGER, J. High-temperature corrosion of superalloys, *Materials Science and Technology*, vol. 3. 1987. pp. 482–493.
6. GURRAPPA, I. Influence of alloying elements on hot corrosion of superalloys and coatings: necessity of smart coatings for gas turbine engines. *Materials Science and Technology*, vol. 19, no. 2. 2003. pp. 178–183.
7. SÜSS, R., HILL, P.J., ELLIS, P. and WOLFF, I.M. The oxidation resistance of Pt-base γ/γ' analogues to Ni-base superalloys. *Proceedings of the 7th European Conference on Advanced Materials and Processes 2001*, CD-ROM ISBN 8885298397.
8. SIDHU, T.S., AGRAVAL, R.D., and PRAKASH, S. Hot corrosion of some superalloys and role of high-velocity oxy-fuel spray coatings-a review. *Surface Coatings and Technology*, vol. 198. 2005. pp. 441–446.
9. HILL, P.J., BIGGS, T., ELLIS, P., HOHLS, J., TAYLOR, S., and WOLFF, I.M. An assessment of ternary precipitation-strengthened Pt alloys for ultra-high temperature applications. *Materials Science and Engineering A*, vol. 301. 2001. pp. 167–179.
10. CORNISH, L.A., SÜSS, R., CHOWN, L.H., TAYLOR, S., GLANER, L., DOUGLAS, A. AND PRINS, S.N. Platinum-based alloys for high temperature and special applications. International Platinum Conference 'Platinum Adding Value', Sun City, South Africa, 3 - 7 October 2004, *South African Institute of Mining and Metallurgy Symposium Series*, S38, pp. 329–336.
11. MÉVREL, R. Cyclic oxidation of high temperature alloys, *Materials Science and Technology*, vol. 3. 1987. pp. 531–536.
12. FISCHER, G., CHAN, W.Y., DATTA, P.K., and BURNELL-GRAY, J.S. Noble metal aluminide coatings for gas turbines. *Platinum Metals Review*, vol. 43, issue 2. 1999. p. 59.
13. POMEROY, M.J. Coatings for gas turbine materials and long term stability issues. *Materials and Design, 2005*, vol 26, issue 3. pp. 223–231.
14. PRAKASH, G.S. and SINGH, S., Effects of MgO and CaO on hot corrosion of Fe base superalloy superfer 800H in Na_2SO_4-60%V_2O_5 environment. *British Corrosion Journal*, vol. 37, no. 1. 2002. pp. 56–62.
15. YOSHIBA, M. Effect of hot corrosion on the mechanical performances of superalloys and coatings systems, *Corrosion Science*, vol. 35, nos. 5–8. 1993. pp. 1115–1124.
16. CHOI, B.K. and LOCKWOOD, D.J. Peculiarities of the structural phase transitions in Na_2SO_2 (V): A Raman scattering study. *J. Physics: Condensed Matter*, vol 17. 2005. pp. 6095–6108.
17. KIM, J.H., and WANG, π, S., Development of an in situ Raman spectroscopic system for surface oxide films on metals and alloys in high temperature water, *Nuclear Engineering and Design*, vol. 235, issue 9. 2005. pp. 1029–1040.
18. DURGA PRASAD, B., SANKARAN, S.N., WIEDEMANN, K. E. and GLASS, D.E. Platinum substitutes and two-phase-glass overlayers as low cost alternatives to platinum aluminide coatings. *Thin Solid Films*, vol. 345. 1999. pp. 255–262.
19. LEE, W.H. and LIN, R.Y., Hot corrosion mechanism of intermetallic compound Ni3Al, *Materials Chemistry and Physics*, vol. 77. 2002. pp. 86–96.